

Relic gravitational waves and their detection

Wen Zhao, Yang Zhang

Astrophysics Center

University of Science and Technology of China

Hefei, Anhui, China

Abstract

As strong evidence for inflation, the relic gravitational waves (RGW) have been extensively studied. Although, it has not been detected, yet some constraints have been achieved by the observations. Future experiments for the RGW detection are mainly two kinds: the CMB experiments and the laser interferometers. In this paper, we study these current constraints and the detective abilities of future experiments. We calculate the strength of RGW $\Omega_g(k)$ in two methods: the analytic method and the numerical method by solving the inflationary flow equations. By the first method we obtain a bound $\Omega_g < 3.89 \times 10^{-16}$ at $\nu = 0.1\text{Hz}$, where we have used the current constraints on the scalar spectral index, the tensor-scalar ratio, furthermore, we have taken into account of the redshift-suppression effect, the accelerating expansion effect, the neutrino damping effect on the RGW. But the analytic expression of $\Omega_g(k)$ depends on the specific inflationary models and only applies for the waves with very low frequencies. The numerical method is more precise for the high frequency waves and applies to any single-field inflationary model. It gives a bound $\Omega_g < 8.62 \times 10^{-14}$, which is independent of the inflationary parameters, and applies to any single-field slow-roll inflationary model. After considering the current constraints on the inflationary parameters, this bound reduces down to $\Omega_g < 2 \times 10^{-17}$. These two methods give the consistent conclusions: The current constraints on the RGW from LIGO, big bang nucleosynthesis, and pulsar timing are too loose to give any stringent constraint for the single-field inflationary models, and the constraint from WMAP are relatively tighter. The future laser interferometers are more effective for detecting the RGW with the smaller tensor-scalar ratio, but the CMB experiments are more effective for detecting the waves with the larger ratio. These detection methods are complementary to each other for the detections of RGW.

PACS numbers: 98.80.-k, 98.80.Es, 04.30.-w, 04.62.+v

e-mail: wzhaoy7@mail.ustc.edu.cn

1. Introduction

In the past, a number of observations on the CMB power spectra [1, 2, 3] and on the large scale structure (LSS) [4] have supported inflation as the good phenomenological model in the sense that it naturally gives rise to the origin of the primordial fluctuations with a nearly scale-invariant and gaussian spectrum. The overall expansion of the Universe at very early stage, as well as the evolution of fluctuations of the perturbed spacetime metric, can be accounted for in the framework of inflationary models. In addition to the primordial density perturbations, inflationary models also predict a stochastic background of RGW, which is the tensorial perturbations of spacetime metric. The detection of such a background would provide incontrovertible evidence that inflation actually occurred and would also set strong constraints on the dynamic of inflation [5].

There are mainly two kinds of experiments to detect RGW at correspondingly different frequencies. For RGW of very low frequencies $\nu \sim 10^{-17} \sim 10^{-15}\text{Hz}$, one can observe them by detecting the power spectrum of CMB B-polarizations [6]. Now, the first-three-year results of WMAP [2] have not yet found the evidence of RGW. The experiment of the Planck satellite [7] with higher sensitivity to polarizations is scheduled for launch in 2007, and the Clover (Cl-Observer) [8] and CMBPol [9] projects with much higher sensitivities than Planck are also under development. For RGW of high frequencies $\nu \simeq 10^{-4} \sim 10^4\text{Hz}$, another kind of experiments apply, i.e. the laser interferometers detectors, including the current TAMA [10], VIRGO [11], LIGO [12, 13], and the future LISA [14], ASTROD [15], BBO [16], and DECIGO [17]. Besides these two kinds, other methods have also been used to constrain the strength of RGW. For example the timing studies on the millisecond pulsars, which can constrain the amplitude of the gravitational waves by studying the signal residuals of the millisecond pulses [18]. This method is sensitive to the waves with frequencies at $10^{-9} \sim 10^{-7}\text{Hz}$. The electromagnetic detectors are based on the processes of resonant responses of electro-magnetic field to incident gravitational waves [19, 20, 21]. This kind of detectors are aiming at detecting RGW at very high frequencies $\nu \sim 10^8 - 10^{10}\text{Hz}$, which can only be produced by inflation [22]. The observational results of BBN also can constrain the strength of RGW [23, 24, 25] at all frequencies. Although the RGW have not been found yet, some constraints on it have already been obtained by these experiments or observations.

This paper is to study the various modifications on the power spectrum of RGW and examine the constraints on it from the experiments. On the spectrum, we will consider the modifications due to such important effects as the redshift-suppression by various periods of cosmic expansions, the current accelerating expansion, and the damping by free-streaming of neutrinos. Two methods will be applied in this study: the analytic method and the numerical method by solving the inflationary flow equations. After considering all these damping effects, we will arrive at an analytic formula of the strength of RGW, which, as a function of the wavenumber k , depends on the scalar spectral index n_s and the tensor-scalar ratio r . By taking into account of the current observational constraints on n_s and r , we will obtain an upper limit of the strength of RGW $\Omega_g < 3.89 \times 10^{-16}$ at $\nu = 0.1\text{Hz}$. From the plots in the $r - \Omega_g$ plane, we find that the BBO experiments can detect the RGW if $r > 8.3 \times 10^{-3}$ is satisfied. This means that BBO is more sensitive than Planck satellite, but less than Clover and CMBPol. But the would-be ultimate DECIGO can even detect for $r > 6.8 \times 10^{-6}$, much more sensitive than the CMB experiments. In this analytic method, Ω_g depends explicitly on the ratio r , an undetermined parameter, whose value varies for the various specific inflationary models. Furthermore, the approximate power law of primordial power spectrum also may yield fairly large error if it is extended over a larger range of frequencies.

To overcome these shortcomings, we move on to the numerical method. Because the RGW depends more sensitively on inflationary stage, during which it is generated, and there are a number of inflationary models, to take care of the predictions from these models, the numerical method is used, by which a great many of realizations are produced, representing the respective inflationary models. The inflationary flow equations are applied to numerically calculate the RGW, whereby an upper limit $\Omega_g < 8.62 \times 10^{-14}$ is obtained for any slow-roll single-scalar-field inflationary model, independent of any inflationary parameters. By taking into account of the current observed constraints on n_s , α , and r , a much tighter limit $\Omega_g < 2 \times 10^{-17}$ is arrived at $r \simeq 0.03$, which is beyond the sensitive range of BBO. In numerically generating 10^7 realizations, we find all of them satisfy the current constraints on Ω_g from LIGO, from pulsar timing, and from BBN, but only nearly 0.05% of them satisfy the current constraints on n_s , α and r . From the resulting $r - \Omega_g$ plane, one finds the DECIGO, if put into running, will be effective for detecting the RGW with smaller r , but the CMB experiments, such as Planck, Clover and CMBPol, are more effective for detecting the RGW with larger r . They are complementary to each other for RGW detections. Our result from this numerical investigation applies only to the single-field inflationary models with the chosen initial conditions of Hubble slow-roll parameters.

The organization of this paper is as follows. Section 2 gives a simply review on the RGW and its evolution equation. In section 3, an analytic expression of the strength of RGW will be obtained with the three damping factors being included, presenting the modifications due to the mentioned effects. Section 4 is devoted to the numerical computations, where the strength of RGW is numerically calculated by solving the inflationary flow

equations. Finally section 5 is the conclusion.

2. The relic gravitational waves and their evolutive equation

Incorporating the perturbations to the spatially flat Robertson-Walker (FRW) spacetime, the metric is

$$ds^2 = a(\tau)^2 [d\tau^2 - (\delta_{ij} + h_{ij})dx^i dx^j] , \quad (1)$$

where a is the scale factor of the universe, τ is the conformal time, which is related to the cosmic time by $ad\tau \equiv dt$. The perturbation of spacetime h_{ij} is a 3×3 symmetric matrix. The gravitational wave field is the tensorial portion of h_{ij} , which is transverse-traceless $\partial_i h^{ij} = 0$, $\delta^{ij} h_{ij} = 0$. Since RGW is very weak, $|h_{ij}| \ll 1$, one needs just study the linearized evolutive equation:

$$\partial_\mu (\sqrt{-g} \partial^\mu h_{ij}) = 16\pi G a^2(\tau) \Pi_{ij} , \quad (2)$$

where Π_{ij} is the tensor part of the anisotropy stress, satisfying $\Pi_{ii} = 0$, and $\partial_i \Pi_{ij} = 0$. It couples to h_{ij} as an external source. In the cosmic setting, Π_{ij} can be generated by the free-streaming relativistic particles [26, 27], the cosmic magnetic [28], etc. It is convenient to Fourier transform these quantities as follows

$$h_{ij}(\tau, \mathbf{x}) = \sum_{\lambda} \sqrt{16\pi G} \int \frac{d\mathbf{k}}{(2\pi)^{3/2}} \epsilon_{ij}^{(\lambda)}(\mathbf{k}) h_{\mathbf{k}}^{(\lambda)}(\tau) e^{i\mathbf{k}\mathbf{x}} , \quad (3)$$

$$\Pi_{ij}(\tau, \mathbf{x}) = \sum_{\lambda} \sqrt{16\pi G} \int \frac{d\mathbf{k}}{(2\pi)^{3/2}} \epsilon_{ij}^{(\lambda)}(\mathbf{k}) \Pi_{\mathbf{k}}^{(\lambda)}(\tau) e^{i\mathbf{k}\mathbf{x}} , \quad (4)$$

where the index $\lambda = “+”$ or $“\times”$ labels the two polarization states of the gravitational waves. The polarization tensors $\epsilon_{ij}^{(\lambda)}$ are symmetry, transverse-traceless $k^i \epsilon_{ij}^{(\lambda)}(\mathbf{k}) = 0$, $\delta^{ij} \epsilon_{ij}^{(\lambda)}(\mathbf{k}) = 0$, and satisfy the conditions $\epsilon^{(\lambda)ij}(\mathbf{k}) \epsilon_{ij}^{(\lambda')}(\mathbf{k}) = 2\delta_{\lambda\lambda'}$ and $\epsilon_{ij}^{(\lambda)}(-\mathbf{k}) = \epsilon_{ij}^{(\lambda)}(\mathbf{k})$. Since the RGW is assumed to be isotropy and each polarization state has the same evolution and gives the same contributions, $h_{\mathbf{k}}^{(\lambda)}(\tau)$ is denoted simply by $h_k(\tau)$, and $\Pi_{\mathbf{k}}^{(\lambda)}(\tau)$ by $\Pi_k(\tau)$, where $k = |\mathbf{k}|$ is the wavenumber related to the frequency by $\nu \equiv k/2\pi$ (the present scale factor is set $a_0 = 1$). Then Eq.(2) can be rewritten as

$$\ddot{h}_k + 2\frac{\dot{a}}{a}\dot{h}_k + k^2 h_k = 16\pi G a^2(\tau) \Pi_k(\tau) , \quad (5)$$

where the overdot denotes a conformal time derivative $d/d\tau$. Usually the interactions between gravitational waves and other matters are very weak, in many cases, the source Π_k in Eq.(5) is negligible, and the evolution of RGW only depends on the scale factor and its time derivative. But in this paper we include this source term, so that the damping from neutrino free-streaming is properly taken care of.

3. The analytic power spectrum of RGW

The primordial power spectrum of RGW

As mentioned in the introduction, inflationary expansion, as an attractive idea to describe the very early universe, has received strong support from the observations of CMB anisotropies and from studies of the large-scale distribution of galaxy. There have been a number of models proposed. Here we will consider only the single field models. In the context of slow-roll inflationary models, the observables depend on three slow-roll parameters [29]

$$\epsilon_V \equiv \frac{M_{\text{Pl}}^2}{2} \left(\frac{V'}{V} \right)^2 , \quad \eta_V \equiv M_{\text{Pl}}^2 \left(\frac{V''}{V} \right) , \quad \xi_V \equiv M_{\text{Pl}}^4 \left(\frac{V'V'''}{V^2} \right) , \quad (6)$$

where $M_{\text{Pl}} \equiv (8\pi G)^{-1/2} = m_{\text{Pl}}/\sqrt{8\pi}$ is the reduced Planck energy, $V(\phi)$ is the inflationary potential, and the prime denotes derivatives with respect to the field ϕ . Here, ϵ_V quantifies “steepness” of the slope of the potential, η_V measures “curvature” of the potential, and ξ_V quantifies the “jerk”. All these three parameters must be smaller than 1 for inflation to occur. One of the important predictions of inflationary models is the primordial scalar perturbation power spectrum, which is nearly gaussian and nearly scale-invariant. This spectrum can be written in the form

$$P_S(k) = P_S(k_0) \left(\frac{k}{k_0} \right)^{n_s(k_0) - 1 + \frac{1}{2}\alpha \ln(k/k_0)} , \quad (7)$$

where n_s is the scalar spectral index, $\alpha \equiv dn_s/d\ln k$ is its running, and k_0 is some pivot wavenumber. In this paper, $k_0 = 0.05\text{Mpc}^{-1}$ is taken, which corresponds to a frequency $\sim 10^{-16}\text{Hz}$. The observations of WMAP gives $P_S(k_0) \simeq 2.95 \times 10^{-9} A(k_0)$ and $A(k_0) = 0.9 \pm 0.1$ [1]. Another major prediction of inflationary models is the existence of RGW. The primordial power spectrum of RGW is defined by

$$P_T(k) \equiv \frac{32Gk^3}{\pi} h_k^+ h_k, \quad (8)$$

where h_k is the solution of the equation in (5). This spectrum can also be put in a simple form

$$P_T(k) = P_T(k_0) \left(\frac{k}{k_0} \right)^{n_t(k_0) + \frac{1}{2}\alpha_t \ln(k/k_0)}, \quad (9)$$

where $n_t(k)$ is the tensor spectral index, and $\alpha_t \equiv dn_t/d\ln k$ is its running. In the single-field inflationary models, a standard slow-roll analysis gives the following relations

$$n_t = -\frac{r}{8}, \quad \alpha_t = \frac{r}{8} \left[(n_s - 1) + \frac{r}{8} \right], \quad r = \frac{8}{3}(1 - n_s) + \frac{16}{3}\eta_V, \quad (10)$$

where $r(k) \equiv P_T(k)/P_S(k)$ is the so-called tensor-scalar ratio. These formulae relate the tensorial parameters n_t and α_t to the scalar parameters n_s and r ; the latter are accessible to the observations of CMB and of LSS. As shown in Eq.(10), the relation between r and n_s involves the slow-roll parameter η_V , depending on the specific inflationary potential. Inserting these into Eq.(9), one has

$$P_T(k) = P_S(k_0) \times r \times \left(\frac{k}{k_0} \right)^{-\frac{r}{8} + \frac{r}{16}[(n_s - 1) + \frac{r}{8}] \ln(k/k_0)}. \quad (11)$$

In general, the tensor-scalar ratio r may vary with the wavenumber k . Here and in the following sections we will take the value of r at $k = k_0$, i.e. $r \equiv r(k_0)$. Now the primordial spectrum of RGW only depends on the parameters n_s and r . The recent constraints by the observations of three-year WMAP, SDSS, SNIa and galaxy clustering [30] are

$$n_s = 0.965 \pm 0.012, \quad (68\% \text{ C.L.}) \quad (12)$$

$$r < 0.22, \quad (95\% \text{ C.L.}) . \quad (13)$$

From the derivation it is obvious that the formula (11) applies properly for in a frequency range around $\sim 10^{-16}\text{Hz}$. The strength of the gravitational waves can be also characterized by the gravitational waves energy spectrum

$$\Omega_g(k) = \frac{1}{\rho_c} \frac{d\rho_g}{d\ln k}, \quad (14)$$

where $\rho_c = 3H_0^2/8\pi G$ is the critical density and $H_0 = 100h \text{ km s}^{-1}\text{Mpc}^{-1}$ is the present Hubble constant (the value $h = 0.72$ is taken through this paper). Ω_g can be related to the primordial power spectrum by the formula [27, 31]

$$\Omega_g(k) = \frac{1}{12H_0^2} k^2 P_T(k) T^2(k), \quad (15)$$

where the transfer function $T(k)$ will take into account of the various damping effects mentioned early, and will be discussed below.

The damping effects

Here three kinds of damping effects will be addressed: First we only consider the redshift-suppression effect caused by the overall expansions of the universe. So temporarily we drop the the anisotropy stress term $\Pi_k(\tau)$ in Eq.(5) due to neutrino free-streaming,

$$\ddot{h}_k + 2\frac{\dot{a}}{a}\dot{h}_k + k^2 h_k = 0. \quad (16)$$

This equation of RGW only depends on the behavior of the scale factor $a(\tau)$. It has been known that, during the expansion of the universe, the mode function $h_k(\tau)$ of the gravitational waves behaves differently in two regimes [22]: far outside the horizon ($k \ll aH$), and deep inside the horizon ($k \gg aH$). When waves are far outside the horizon, the amplitude of h_k keeps constant, and when inside the horizon, the amplitude is damping with the expansion of the universe

$$h_k \propto \frac{1}{a(\tau)}. \quad (17)$$

By numerically integrating the Eq.(16), this effect can be approximately described by a transfer function [32]

$$t_1(k) = \frac{3j_1(k\tau_0)}{k\tau_0} \sqrt{1.0 + 1.36 \left(\frac{k}{k_{eq}}\right) + 2.50 \left(\frac{k}{k_{eq}}\right)^2}, \quad (18)$$

where $k_{eq} = 0.073\Omega_m h^2 \text{Mpc}^{-1}$ is the wavenumber corresponding to the Hubble radius at the time that matter and radiation have equal energy densities. And $\tau_0 = 1.41 \times 10^4 \text{Mpc}$ is the present conformal time. It is obvious that, this factor $t_1(k)$ is oscillating with wavenumber k due to the Bessel function $j_1(k\tau_0)$. In practice, one is usually interested in the overall outline of the amplitude of RGW, as the quick oscillations with k are of no importance. For the waves with $k\tau_0 \gg 1$, this factor can be written as

$$t_1(k) = \frac{3}{(k\tau_0)^2} \sqrt{1.0 + 1.36 \left(\frac{k}{k_{eq}}\right) + 2.50 \left(\frac{k}{k_{eq}}\right)^2}. \quad (19)$$

The above transfer function (19) does not include the effect of accelerating expansion of the present universe, which has been indicated by the observations on SN 1a. The spectrum of RGW has been studied in specific models for dark energy [33], such as the Chaplyngin gas models and the X-fluid model. In the Ref.[22], we have presented an analytic solution of RGW in Λ CDM universe, and found that the amplitude of the gravitational waves has been modified by the presence of the dark energy during the current expansion. In the higher frequency range ($\nu \gg 3 \times 10^{-18} \text{Hz}$) that we are interested in this paper, the amplitude acquires an overall factor Ω_m/Ω_Λ as compared with the decelerating model, where Ω_m and Ω_Λ are the present energy densities of matter and vacuum, respectively. So this effect can be simply described by a damping factor,

$$t_2 = \frac{\Omega_m}{\Omega_\Lambda}. \quad (20)$$

In the standard Λ CDM model with $\Omega_m = 0.27$ and $\Omega_\Lambda = 0.73$, this effect contributes a damping factor of $t_2^2 \sim 0.137$ for the strength of RGW in Eq.(15).

The third to be considered is the damping effect of the free-streaming neutrinos [26], i.e. the anisotropic stress Π_k on the right-hand of the Eq.(5). This effect has been considered by Weinberg [26]. This effect is primarily produced by neutrinos during the radiation dominated era when they are decoupled and are free streaming in the universe, especially right after the gravitational waves enter the horizon. The overall amplitude of RGW will reduce roughly by an amount of 20%. It has been shown that anisotropy stress can reduce the amplitude for the wavelengths that re-enter the horizon during the radiation-dominated stage, and the damping factor is only dependent on the fraction f of the free-streaming relativistic particles over the background (critical) energy density in the universe. For the waves that enter the horizon at later times, the damping effect is less important. A number of works have done to discuss this effect, and Reference [27] has found that the effect can be approximately described by a transfer function t_3 for the waves with wavenumbers $k > 10^{-16} \text{Hz}$ (which re-enter the horizon at the radiation-dominant stage),

$$t_3 = \frac{15(14406f^4 - 55770f^3 + 3152975f^2 - 48118000f + 324135000)}{343(15 + 4f)(50 + 4f)(105 + 4f)(180 + 4f)}. \quad (21)$$

When the wave modes ($10^{-16} \text{Hz} < k < 10^{-10} \text{Hz}$) re-enter the horizon, the temperature in the universe is relatively low ($< 1 \text{MeV}$), the neutrino is the only free-streaming relativistic particle. Thus we choose the fraction $f = 0.4052$, corresponding to 3 species of neutrinos in the standard model, the damping factor is then $t_3 = 0.80313$. But for the waves with very high frequency ($k > 10^{-10} \text{Hz}$), the temperature of the universe is still very high when they re-enter the horizon, the neutrinos were still in interaction, and the value of f is quite uncertain. This is because the detail of how many species of particles are free is not accurately known and depends on the cosmic environment and the particle-interaction models. Thus, the detection of RGW at this range of frequencies offers the possibility of learning more about the free-streaming fraction f in the very early universe. So we choose $f = 0$, i.e. there are no free-streaming relativistic particle at that time. The corresponding factor is then $t_3 = 1$. But for the waves with $k < 10^{-16} \text{Hz}$, which re-enter the horizon during the matter-dominated stage, the neutrino density is so small that its damping impact can be neglected, so we choose $t_3 = 1$. Overall, the neutrino damping effect can approximately be summarized as

$$t_3(k) \simeq \begin{cases} 1, & k < 10^{-16} \text{Hz} \\ 0.80313, & 10^{-16} \text{Hz} < k < 10^{-10} \text{Hz} \\ 1, & k > 10^{-10} \text{Hz}. \end{cases} \quad (22)$$

Putting these three effects together, the total transfer function is the combination of three factors

$$T(k) = t_1 \times t_2 \times t_3, \quad (23)$$

among these t_1 is dominantly important, which approximately shows the evolution of RGW in the expanding universe. The function t_2 has the relatively smaller damping on RGW, which accounts for the accelerating expansion of the universe quite recently ($z \sim 0.3$). The value of energy spectrum Ω_g is reduced by nearly an order by this effect. The function of t_3 has the most uncertainty, as has been discussed above. In the extreme case with $f = 0$, one has $t_3 = 1$, i.e. no damping; and in another extreme case with $f = 1$, one has $t_3 = 0.35$, the smallest value of t_3 . In the case of $f = 0.4052$, $t_3 = 0.80313$, only contributing a damping factor $t_3^2 = 0.645$ for the strength of the RGW.

There are some other possible mechanisms, which might affect the amplitude of the gravitational waves. For example, the QCD transition [34, 35], e^+e^- annihilation [34, 36, 35], the cosmic reheating [37, 22], and so on [27]. These could influence the value of expansion rate \dot{a}/a , and therefore affect the strength of RGW. However, these effects are either small, as shown in literature, in comparison with the effects we have discussed, or there are some uncertainties in their analysis, so these are not considered in here.

The upper limit of Ω_g and the sensitivities of future experiments

The future detectors of RGW are mainly classified into two kinds: one kind is through CMB for very low frequencies, and another is based on laser interferometers for relatively high frequencies.

For the waves of very low frequencies $\nu < 10^{-15}\text{Hz}$, the CMB experiments are sensitive. For instance, the Planck satellite can detect the RGW if $r > 0.1$ [7], the ground-based experiment Clover can detect the signal if $r > 0.005$ [8], and CMBPol can detect if $r > 10^{-3}$ is satisfied [9]. It should notice that if $r < 1 \times 10^{-4}$, the RGW may not be detected by the CMB experiments. This is because the CMB B-polarizations generated by the cosmic lensing are also very large, and the signals from the RGW may be subdominant to the lensing effects. [38].

The direct detections the RGW by laser interferometers are sensitive to the waves with high frequencies. For the waves with $k > 10^{-10}\text{Hz}$, inserting the formulas (19)-(23) with $t_3 = 1$ in Eq.(15), the strength of the gravitational waves becomes

$$\Omega_g(k) = \frac{22.5}{12H_0^2} \frac{P_T(k)}{\tau_0^4 k_{eq}^2} \left(\frac{\Omega_m}{\Omega_\Lambda} \right)^2 \simeq 1.08 \times 10^{-6} P_T(k) \quad , \quad (24)$$

Using the expression of $P_T(k)$ in Eq.(11), one gets

$$\Omega_g(k) \simeq 2.87 \times 10^{-15} r \left(\frac{k}{k_0} \right)^{-\frac{r}{8} + \frac{r}{16} [(n_s - 1) + \frac{r}{8}] \ln(k/k_0)} \quad , \quad (25)$$

where $A(k_0) = 0.9$ has been taken. This function depends on the wavenumber k , the tensor-scalar ratio r and the scalar spectral index n_s . It should be pointed out that, just as Eq.(11), this formula (25) also applies properly in a frequency range around $\sim 10^{-16}\text{Hz}$.

The advanced LIGO can detect the waves with $\Omega_g h^2 > 10^{-9}$ at $\nu \simeq 100\text{Hz}$ [13]. The LISA project is expected to detect waves with $\Omega_g h^2 > 10^{-11}$ at $\nu \simeq 0.005\text{Hz}$ [14]. The ASTROD, a space project sensitive to the waves with frequency at $\nu \in (10^{-5}, 10^{-3})\text{Hz}$ [15], is expected to detect the waves with $\Omega_g h^2 > 10^{-15}$ at $\nu \simeq 5 \times 10^{-4}\text{Hz}$. The BBO, another important project, can detect a background RGW with $\Omega_g > 2.2 \times 10^{-17}$ at $\nu \simeq (0.1-1)\text{Hz}$ [16]. The DECIGO project, having a much higher sensitivity by design, is expected to detect the RGW with $\Omega_g h^2 > 10^{-20}$ at $\nu \simeq 0.1\text{Hz}$ [17].

First, we will estimate the upper limit on the strength of RGW in Eq.(25). Here we assume $n_s \leq 1$ and $r < 0.22$, which are consistent with the current observations [30]. The formula (25) gives an upper limit of Ω_g at $\nu = 0.1\text{Hz}$:

$$\Omega_g < 3.89 \times 10^{-16} \quad . \quad (26)$$

And this limit is arrived at $n_s = 1$ and $r = 0.22$. This limit is nearly an order smaller than the result in Ref.[31]. This is because our analysis has taken into account of the damping effect of the accelerating expansion of the universe and the running of n_t in the primordial spectrum. This limit is in the sensitive ranges of BBO and DECIGO, but beyond those of LIGO, LISA and ASTROD. In Fig.[1], we plot the strength of RGW at $\nu = 0.1\text{Hz}$, as the function of r , where several models with different n_s are demonstrated. One sees that when $r < 0.01$, the curves of the function Ω_g are almost overlapped for the models of different n_s , and only depend on the variable r . But when $r > 0.01$, the models of different n_s can be distinguished. For a fixed r , a larger n_s yields a larger Ω_g . This figure also tells that BBO can detect the RGW if $r > 8.3 \times 10^{-3}$, so it is more sensitive than the Planck satellite, but less than Clover and CMBPol. It is interesting to notice that DECIGO can detect the RGW if $r > 6.8 \times 10^{-6}$, which is much more sensitive than all the CMB experiments ($r > 10^{-4}$).

The predictions of inflationary models

The strength of RGW in Eq.(25) depends on the values of n_s and r . Observations have yielded quite solid constraints on n_s , but the value of r is still uncertain. The relation between n_s and r depends on the specific

inflationary models, and different models will predict very different r . In the following examinations will made for several inflationary models, which predict different values of r . One may categorize slow-roll models into several classes according to the parameter space spanned by n_s , α and r [39]. Each class should correspond to specific physical models of inflation. Here we categorize the models according to the curvature of potential η_V in Eq.(6), as it is the only parameter that enters into the relation (10) between n_s and r . The classes are defined in the following:

Case A: negative curvature models $\eta_V < 0$

The negative η_V models often arise from a potential of spontaneous symmetry breaking. One type of often-discussed potentials have the form of $V = \Lambda^4 [1 - (\phi/\mu)^p]$, where $p \geq 2$. This kind of models predict the red tilt $n_s < 1$, which is consistent with the observations of three-year WMAP. Also these models predict pretty small r . For the model with $p = 2$ in Ref.[39],

$$r \simeq 8(1 - n_s)e^{-N(1-n_s)}, \quad (27)$$

where N is the number of e-folds, taken be in the range $N \in [40, 70]$ to account for the current observations on CMB [40, 1, 2]. Here we choose the value $N = 70$. Using the constraint on n_s in Eq.(12) yields the constraint $r \in [0.014, 0.037]$. From Fig.[1], one finds this is beyond the sensitive range of the Planck satellite, but in the sensitive ranges of Clover, and CMBPol. And it is also in the sensitive range of BBO and DECIGO. In other models with $p > 2$, the predicted values of r are much smaller than that of the model with $p = 2$.

Case B: small positive curvature models $0 \leq \eta_V \leq 2\epsilon_V$

These models contain as two examples the monomial potentials $V = \Lambda^4(\phi/\mu)^p$ with $p \geq 2$ for $0 < \eta_V < 2\epsilon_V$ and the exponential potential $V = \Lambda^4 \exp(\phi/\mu)$ for $\eta_V = 2\epsilon_V$. In these models, to the first order in slow roll, the scalar index is always red $n_s < 1$ and the following constraint on r is satisfied

$$\frac{8}{3}(1 - n_s) \leq r \leq 8(1 - n_s). \quad (28)$$

Using the constraint on n_s in Eq.(12), one finds that $r \in [0.061, 0.376]$, which is in the sensitive ranges of Clover, CMBPol, BBO, and DECIGO. The sensitivity limit of Planck is just in this span, so it may be able to detect the model.

Case C: intermediate positive curvature models $2\epsilon_V < \eta_V \leq 3\epsilon_V$

The supergravity-motivated hybrid models have a potential of the form $V \simeq \Lambda^4 [1 + \alpha \ln(\phi/Q) + \lambda(\phi/\mu)^4]$, up to one-loop correction during inflation. In this case,

$$n_s < 1, \quad r > 8(1 - n_s), \quad (29)$$

are satisfied. Using the constraint on n_s in Eq.(12), one finds that $r > 0.184$, which is very close to the current upper limit $r < 0.22$. Fig.[1] shows that this model is in the sensitive range of Planck satellite.

Case D: large positive curvature models $\eta_V > 3\epsilon_V$

This class of models have a typical monomial potential similar to the Case A, but with a plus sign for the term $(\phi/\mu)^p$: $V = \Lambda^4 [1 + (\phi/\mu)^p]$. This will enable inflation to occur for a small value of $\phi < m_{\text{Pl}}$. This model predicts a blue tilt of scalar index $n_s > 1$, which is contradict to the constraint in Eq.(12). But we should notice that the observations of three-year WMAP has not yet ruled out the blue spectrum. If the the running of n_s with the wavenumber k is allowed, then the best fit of WMAP data suggests that $n_s(k = 0.002\text{Mpc}^{-1}) = 1.21^{+0.13}_{-0.16}$, and $\alpha(k = 0.002\text{Mpc}^{-1}) = -0.102^{+0.050}_{-0.043}$ [2]. This is a blue spectrum with a negative running. So the determination of the value of n_s depends on the more precise observations.

4. The inflationary flow equations and the predictions for RGW

In the discussions, the RGW given by the analytic expression (25) depends on the value of tensor-scalar ratio r , which has not yet been determined by the observations. Moreover, Eq.(25) is a good approximation only for the waves with wavenumber around $k \simeq k_0 (\sim 10^{-16}\text{Hz})$. Therefore, for the waves of high frequencies, say with $\nu \simeq 0.1\text{Hz}$, nearly 15 orders larger than the value of k_0 , direction application of the formula (25) may lead to large errors. Consequently, it will be restricted in practice. To avoid these shortcomings, in this section, we will employ the technique of the inflationary flow equations to relate RGW in lower frequencies to that in higher frequencies.

The inflationary flow equations

The inflationary flow equations were first introduced by Hoffman and Turner [41] as a way of generating a large number of slow-roll inflationary models to be compared to the observational data. This method applies to any slow-roll single scalar field inflationary models, and relies on defining a set of Hubble slow-roll parameters, which are

the derivatives of the Hubble parameter during inflation. The major advantage of this method is that it removes the field from the dynamics, and allows one to study the generic behavior of slow-roll inflation without making detailed assumptions about the underlying particle physics. In this section, we will also use this method to generate a large number of inflationary models, the observables of which are required to be consistent with the current observational constraints in low frequencies. Then we will numerically solve the strength of RGW in very high frequencies. In this method the Hubble slow-roll parameters are defined by

$$\epsilon(\phi) \equiv \frac{m_{\text{Pl}}^2}{4\pi} \left(\frac{H'(\phi)}{H(\phi)} \right)^2, \quad \lambda_l(\phi) \equiv \left(\frac{m_{\text{Pl}}^2}{4\pi} \right)^l \frac{(H')^{l-1}}{H^l} \frac{d^{(l+1)}H}{d\phi^{(l+1)}}, \quad (l \geq 1), \quad (30)$$

where primes are derivatives with respect to the scalar field ϕ , and $H(\phi)$ is the Hubble parameter as the function of ϕ , related to the potential $V(\phi)$ by the so-called Hamilton-Jacobi formula,

$$[H'(\phi)]^2 - \frac{12\pi}{m_{\text{Pl}}^2} H^2(\phi) = -\frac{32\pi^2}{m_{\text{Pl}}^4} V(\phi). \quad (31)$$

These Hubble slow-roll parameters satisfy an infinite set of hierarchical differential equations, called inflationary flow equations:

$$\frac{d\epsilon}{dN} = \epsilon(\sigma + 2\epsilon), \quad (32)$$

$$\frac{d\sigma}{dN} = -\epsilon(5\sigma + 12\epsilon) + 2(\lambda_2), \quad (33)$$

$$\frac{d}{dN} \lambda_l = \left[\frac{l-1}{2} \sigma + (l-2)\epsilon \right] \lambda_l + \lambda_{l+1}, \quad (l \geq 2) \quad (34)$$

where N is the number of e -folds of the inflation, and $\sigma \equiv 2\lambda_1 - 4\epsilon$. There are two families of fixed points of these flow equations: One is that $\epsilon = 0$, $\lambda_l = 0$ for $l \geq 2$, and $\sigma = \text{constant}$. In Ref.[42], the authors found that, only if $\sigma > 0$, this fixed point is stable, i.e. the attractor solution. The other family of fixed points are given by: $\epsilon = \text{constant}$, $\sigma = -2\epsilon$, $\lambda_2 = \epsilon^2$, and $\lambda_l = \epsilon\lambda_{l-1}$ for $l \geq 3$. Later we will show that the second family of fixed points is not stable. The slow-roll parameters tend to run to the attractor with the expansion of the universe, as long as the slow-roll condition $\epsilon < 1$ is satisfied. In order to actually solve this infinite series of equations numerically, it must be truncated at some l by setting a sufficiently high slow-roll parameter to zero, i.e. $\lambda_{m+1} = b$, with b being a constant, and $\lambda_{m+2} = 0$ for some suitably large m . In this section, we make the truncation of this series at $m=10$, and choose a set of acceptable initial conditions as in Refs.[42, 31]:

$$\epsilon|_i \in [0, 0.8], \quad (35)$$

$$\sigma|_i \in [-0.5, 0.5], \quad (36)$$

$$\lambda_2|_i \in [-0.05, 0.05], \quad (37)$$

$$\lambda_l|_i \in [-0.025 \times 5^{-l+3}, 0.025 \times 5^{-l+3}], \quad (3 \leq l \leq 10), \quad (38)$$

where the subscript $|_i$ denote the corresponding initial values. This set of eleven equations in Eqs.(32)-(34) is an autonomous system [42]. We choose the constant $b \neq 0$, and set the left hand of these equations to be zero. Then the only real solution for this eleven-equation set is given by

$$\epsilon_c = b^{1/11}, \quad \sigma_c = -2b^{1/11}, \quad \lambda_{lc} = b^{l/11}, \quad (2 \leq l \leq 10), \quad (39)$$

where the subscript c means the fixed point. This is just the second family of fixed points with $\epsilon_c = b^{1/11}$. As usual, in order to study the stability of this fixed points, let us consider the small perturbations around the fixed point, i.e.

$$\epsilon = \epsilon_c + \delta\epsilon, \quad \sigma = \sigma_c + \delta\sigma, \quad \lambda_l = \lambda_{lc} + \delta\lambda_l, \quad (2 \leq l \leq 10). \quad (40)$$

Substituting these into Eqs.(32)-(34), one gets the first-order differential equations for the small perturbations

$$\frac{d}{dN} \begin{pmatrix} \delta\epsilon \\ \delta\sigma \\ \cdot \\ \cdot \\ \delta\lambda_{10} \end{pmatrix} = M \begin{pmatrix} \delta\epsilon \\ \delta\sigma \\ \cdot \\ \cdot \\ \delta\lambda_{10} \end{pmatrix}, \quad (41)$$

where the matrix M depends upon the values of ϵ_c , σ_c and λ_{lc} , $l = 2, \dots, 10$. If this fixed point is stable, at least, it is necessary that the real parts of the eigenvalues of the matrix M are negative [43]. We have performed calculations and found that no matter what value of $b \neq 0$ is chosen, this condition can not be satisfied. Therefore, this fixed point is not stable. If we choose the value $b = 0$, this eleven-equation set in Eqs.(32)-(34) has fixed points, which belong to the first family mentioned early and are stable only if $\sigma_c > 0$ is satisfied.

It is obvious that the evolutions of this eleven-equation set will be different for the conditions with different b . Although whether the fixed points are stable or not depends on the value of $b = 0$, still in the computation below, we will do computations for both kinds of initial conditions: one with $b = 0$, and the other $b \neq 0$ with

$$b \in [-0.025 \times 5^{-8}, 0.025 \times 5^{-8}] . \quad (42)$$

It will turn out that, for these two cases, our calculational results of Ω_g are very similar. So in the following sections, we will only present the results of the $b = 0$ case.

The inflationary parameters and the strength of RGW

Many observable parameters in inflationary models can be related to the . Here we are only interested in three such kind of observable parameters for the slow-roll inflationary models: the tensor-scalar ratio r , the scalar spectral index n_s , and its running α . They are related to the Hubble slow-roll parameters as the following (up to the second order in the slow-roll) [44]

$$r \simeq 16\epsilon[1 - c(\sigma + 2\epsilon)] , \quad (43)$$

$$n_s \simeq 1 + \sigma - (5 - 3c)\epsilon^2 - \frac{1}{4}(3 - 5c)\sigma\epsilon + \frac{1}{2}(3 - c)\lambda_2 , \quad (44)$$

$$\alpha = -\frac{1}{1 - \epsilon} \frac{dn_s}{dN} , \quad (45)$$

where $c = 4(\ln 2 + \gamma) - 5 \simeq 0.0814514$ (with γ the Euler-Mascheroni constant) is a constant. Once the inflationary flow equations in (32)-(34) are numerically solved, the values of these three observables are obtained. As we have pointed out early, we are interested for the gravitational waves in a very wide frequency range, $\nu \in [10^{-16}, 10^2]\text{Hz}$, and the primordial power spectrum in Eq.(9), as an analytic approximation, may not apply properly. Therefore, we need to adopt the following primordial power spectrum[45]

$$P_T(k) = \frac{16}{\pi} \left[1 - \frac{c+1}{4}\epsilon \right]^2 \frac{H^2}{m_{\text{Pl}}^2} \Big|_{k=aH} , \quad (46)$$

which is proper for the slow-roll inflationary models in general. Here H is the Hubble parameter of inflation when the waves exactly crossed the horizon with $k = aH$. If one ignored the small slow-roll parameter ϵ in Eq.(46), then one would end up with $P_T(k) = \frac{16}{\pi} \frac{H^2}{m_{\text{Pl}}^2} \Big|_{k=aH}$, a result for the exact de Sitter inflation, depending only on the Hubble parameter H . The formula (46) can be rewritten as

$$P_T(k) = \left(\frac{4 - (c+1)\epsilon}{4 - (c+1)\epsilon_i} \right)^2 \frac{H^2}{H_i^2} P_T(k_0) , \quad (47)$$

where ϵ_i and H_i are the respective values of ϵ and H when k_0 just crosses the horizon at $a = k_0/H_i$. By the way, the RGW power spectrum can be related to the scalar one by $P_T(k_0) = P_S(k_0)r(k_0)$ as before. The value of H is also related to H_i through the parameter ϵ by the following

$$H(N) = H_i \exp \left[- \int_{N_i}^N \epsilon(n) dn \right] , \quad (48)$$

where N_i is the number of e-folds if $H = H_i$. Inserting the Eqs.(47) and (48) into Eq.(15), one obtains the energy spectrum of RGW

$$\Omega_g(k) = 2.21 \times 10^{-10} r \left(\frac{k}{H_0} \right)^2 T(k)^2 \left(\frac{4 - (c+1)\epsilon}{4 - (c+1)\epsilon_i} \right)^2 \exp \left[-2 \int_{N_i}^N \epsilon(n) dn \right] , \quad (49)$$

where $T(k)$ is the damping factor, and H_0 is the present Hubble constant. Making use of $T(k)$ as given in Eqs.(19), (20), (21) and the ratio r in Eq.(43), one converts the above energy spectrum of RGW into the following form

$$\Omega_g(k) \simeq 4.59 \times 10^{-14} [\epsilon_i - c(\sigma_i \epsilon_i + 2\epsilon_i^2)] \left(\frac{4 - (c+1)\epsilon}{4 - (c+1)\epsilon_i} \right)^2 \exp \left[-2 \int_{N_i}^N \epsilon(n) dn \right] , \quad (50)$$

which now depends only on the slow-roll parameters ϵ and σ . As an advantage to Eq.(25), this spectrum is good also for the waves with $\nu \gg 10^{-10}\text{Hz}$. Before numerically computing it through the inflationary flow equations, we first give an estimate of its upper limit. Since $0 \leq \epsilon < 1$ is satisfied during the inflation, Eq.(50) yields the upper limit when taking $\epsilon = 0$

$$\Omega_g(k) < 7.34 \times 10^{-13} \frac{\epsilon_i - c(\sigma_i \epsilon_i + 2\epsilon_i^2)}{(4 - (c+1)\epsilon_i)^2}, \quad (51)$$

depending on the values of ϵ_i and σ_i . When $\epsilon_i = 1$, the right-hand of this inequality has the maximum value, so one can give a loose upper limit of $\Omega_g(k)$:

$$\Omega_g(k) < 8.62 \times 10^{-14}, \quad (52)$$

where the approximation $r \simeq 16\epsilon$ has been used, and the second-order terms of the tensor-scalar ratio r have been omitted. This upper limit holds only if the slow-roll condition is satisfied. Compared with the limit in Eq.(26), this upper limit is arrived at without explicitly using the values of n_s and r . Besides, this limit applies for a wider range of frequencies $\nu > 10^{-10}\text{Hz}$. It is seen that this limit is much less stringent than that in Eq.(26). Still the limit (52) is much smaller than the sensitivity of, and therefore can not be directly detected by LIGO and LISA, however, it is now larger than the sensitivity of, and can be detected by ASTROD, BBO and DECIGO. In writing down the limit (52), $t_3 = 1$ has been used, which is valid for waves with $\nu \gg 10^{-10}\text{Hz}$. But for the waves with $\nu \in [10^{-16}, 10^{-10}]\text{Hz}$, one should use $t_3 \simeq 0.80313$, and thus the limit becomes $\Omega_g(k) < 5.56 \times 10^{-14}$, which is a little tighter than the limit in Eq.(52).

The current constraints on the cosmic parameters

Through the discussion above, we know that the values of the inflationary parameters n_s , α , r , and Ω_g are all directly related to the Hubble slow-roll parameters. Here, we give a review of the current constraints on them. The constraints on n_s , α and r mainly come from the observations on large scales, including the observations of CMB, LSS and so on. Here we call them as “large-scale constraints” (LSC). When solving the inflationary flow equations, we will take the initial condition at the time of horizon-leaving, i.e. $k_0 = aH$, where the pivot wavenumber $k_0 = 0.05\text{Mpc}^{-1}$ as before.

Now the WMAP CMB data (1st year) gives [1] $n_s = 0.93 \pm 0.07$, $\alpha = -0.047 \pm 0.040$, and the best fit of WMAPext+2dFGRS galaxy survey gives $n_s = 0.93 \pm 0.03$, $\alpha = -0.031^{+0.016}_{-0.017}$. A fit using WMAP CMB data and the SDSS galaxy survey gives [46] $n_s = 0.98 \pm 0.02$, $\alpha = -0.003 \pm 0.010$. Combining the observations of three-year WMAP, SDSS, SNIa and galaxy clustering [30], one can give the constraints $n_s = 0.965 \pm 0.012$, $\alpha = -(2.0 \pm 1.2) \times 10^{-2}$ and $r < 0.22$. These bounds of n_s and α are all at the 68% confidence level, and that of r is at 95% confidence level. These various bounds are consistent with each other, taking into account of the corresponding confidence levels. Here in our calculation we will choose the most loose constraints

$$n_s \in [0.86, 1.00], \quad \alpha \in [-0.087, 0.007], \quad r < 0.22. \quad (53)$$

which imply that the primordial scalar spectrum is “red” or scale-invariant, and the running of scalar index is very small, as required by the slow-roll inflationary models.

The constraints on Ω_g mainly come from the observations at small scale. Here we call them as “small-scale constraints” (SSC), which include the tightest constraint from the observations of the pulsar timing [18]

$$\Omega_g h^2 < 2 \times 10^{-9}, \quad \nu = 1.9 \times 10^{-9} \text{Hz}; \quad (54)$$

the constraint from the recent observations of LIGO [12],

$$\Omega_g < 8.4 \times 10^{-4}, \quad 69 \text{Hz} < \nu < 156 \text{Hz}; \quad (55)$$

and the constraint from the observations of BBN [23, 24],

$$w_g h^2 < 8.9 \times 10^{-6}, \quad (56)$$

where $w_g \equiv \int \Omega_g(\nu) d \ln \nu$. Comparing with the constraints (26) and (52), it is fair to say that the current SSC are too loose to give any constraint on the single-field inflationary models. This result will also be checked in the following numerical calculation.

The distribution of the realizations

In this part, we will present a numerical program to solve the inflationary flow equations (32)-(34) for a large number of models, where each initial condition randomly chosen within the constraints of (35)-(38) will represent an inflationary model.

First, we want to study how tight the LSC of Eq.(53) and SSC of Eqs.(54)-(56) are, as constraints, on the inflationary models. We have produced 10^7 realizations of inflationary models. It turns out that all these realizations satisfy the SSC, which attests to the conclusion before: the current SSC are too loose to give any actual constraint on the single-field inflationary models. On the other hand, among these 10^7 realizations, only 5523 of them ($\sim 0.05\%$) satisfy the LSC of Eq.(53). So this constraint is tighter for the inflationary models. In the following, we will mainly discuss the distribution of these 5523 realizations.

During the numerical calculations, the inflation can end in one of the following two ways. One is that $\epsilon < 1$ is violated in the process of computing, then the inflation automatically stopped. A number of inflationary models are of this class, such as the polynomial “large-field” models, the “small-field” polynomial potentials [39]. The other way is by an abrupt termination, perhaps from intervention of an auxiliary field as in hybrid inflation. The linear potentials and the exponential potentials also belong to this class [39]. Here we choose the abrupt stop to be at $N = 70$ in computation. We have found that among these 5523 realizations, only 14 of them stop the inflation in the first way, all others do in the second way. This fact is consistent with the previous works [42, 31]. In following we will discuss these two kinds of realizations separately.

First, we discuss the 5509 realizations that exit inflation by abrupt termination. They also satisfy both the large and small scale constraints in Eqs.(53)-(56). These models can inflate at least 70 e-folds. In Fig.[2], we plot them in the $r - \Omega_g$ plane, which shows the following characters:

- a. For a fixed r , the distribution of Ω_g is very scattered, especially at the region with large r . For example, for a fixed $r = 0.22$, the values of Ω_g are distributed in a broad range $\Omega_g \in [10^{-45}, 10^{-20}]$;
- b. For each fixed r , the values of Ω_g have an upper limit, and the small region just below this limit tend to contain most of the realizations;
- c. For each fixed r , the values of the upper limit Ω_g from our numerical result are smaller than the analytic results of Eq.(25), especially in the region $r > 0.01$;
- d. At $r \simeq 0.03$, the strength of RGW attains the maximum value $\Omega_g \simeq 2 \times 10^{-17}$, which is almost an order of magnitude smaller than the analytic result of Eq.(26). And this is beyond the sensitive ranges of LIGO, LISA, ASTROD and BBO.
- e. Most of the realizations tend to concentrate in the region with the large values of r , and the larger r is, the denser the distribution of the realizations are. More than 90% of realizations are in the region of $r > 0.01$. This phenomenon of distribution may be due to our specific choice of the initial conditions in Eq.(35)-(38).

Among these 5509 realizations, 50.21% fall into the sensitivity region of the Planck satellite, 97.11% fall into that of Clover, 99.29% fall into that of CMBPol, and 42.91% fall into the sensitivity region of the DECIGO. In comparison with the CMB observations, much less realizations are in the sensitivity regions of laser interferometer detectors. But DECIGO can detect the RGW with r being much smaller than 10^{-4} , which is beyond the CMB experiments. This conclusion is the same as the analytic results in section 3. Therefore, the CMB experiments and the laser interferometers are complementary to each other for the RGW detection.

Now let us look at the 14 realizations that satisfy all the constraints in Eqs.(53)-(56), but end the inflation before the e-folds $N = 70$ arrived. We found, for these realizations, the values of e-folds are all in the region of $N \in [40, 70]$, which is consistent with the current observations and the theoretic predictions [39]. In Fig.[3], we plot them in the $r - \Omega_g$ plane. This figure shows an interesting feature: larger r corresponds to a smaller Ω_g , which is also consistent with the distribution of realizations in Fig.[2]. Among these realizations, 35.71% fall into the sensitive region of the Planck satellite, 100% fall into the sensitive regions of Clover and CMBPol, and 64.29% fall into the sensitive region of the DECIGO. These results are also consistent with the distribution of the 5509 realizations discussed in the above.

It should be mentioned that, in our numerical calculation, the initial conditions have been chosen randomly for the Hubble slow-roll parameters in the regions (35)-(38). It is not clear which one is closer to the actual situation of the inflationary process in the early Universe. However, given the very broad range of initial conditions for the Hubble slow-roll parameters, these large sample of 10^7 realizations may exhaust, to some extent, the reasonable reservoir of inflationary models driven by the single scalar field.

5. Conclusion

The relic gravitational waves is regarded as a strong evidence for the inflationary models, which is directly related to the energy scale of the inflation. Although up to now people have not observed RGW, a lot of constraints have been obtained on them. These constraints include two kinds: One is the LSC, which are mainly from the CMB observations, especially the recent WMAP results. This can constrain the RGW at very low frequency $\nu \in [10^{-17}, 10^{-15}]$ Hz. The other is the SSC, mainly from LIGO, BBN, and pulsar timing, and it is sensitive to the waves with high frequencies. A number of experiments are under development for the RGW detection, which can be classified as the following types: the CMB experiments (sensitive to the waves with $\nu \in [10^{-17}, 10^{-15}]$ Hz), including

Planck, Clover, CMBPol, etc, the laser interferometers (sensitive to the waves with $\nu \in [10^{-4}, 10^4]\text{Hz}$), including advanced LIGO, LISA, ASTROD, BBO, DECIGO, etc, the electromagnetic detectors (sensitive to the waves with $\nu \in [10^8, 10^{10}]\text{Hz}$).

We have calculated the strength of RGW, studied how tight of the current constraints on the RGW, and examined the detective abilities of the future experiments. When calculating the values of $\Omega_g(k)$, we have worked in two methods: the analytic and the numerical. The former method simply shows the dependent relation of $\Omega_g(k)$ on the inflationary parameters n_s and r . After considering the current constraints on these parameters, we have given an upper limit $\Omega_g < 3.89 \times 10^{-16}$, where the three damping effects have been included, such as the reashift-suppression, the accelerating expansion, and the free-streaming neutrinos. This limit is in the sensitivity ranges of BBO and DECIGO, but beyond which of advanced LIGO, LISA and ASTROD. In the numerical method, the energy spectrum $\Omega_g(k)$ has been calculated by solving the inflationary flow equations. The resulting spectrum is more precise for the RGW at high frequency range. The corresponding upper limit $\Omega_g < 8.62 \times 10^{-14}$ has been given, which is independent of the inflationary parameters and applies to any single-field slow-roll inflationary model. After considering the constraints on n_s , α and r , this bound becomes $\Omega_g < 2 \times 10^{-17}$, which is beyond the sensitivity limit of BBO.

The results from these two methods suggest the consistent conclusions: The current constraints on the RGW from LIGO, BBN and pulsar timing are too loose to give any constraint for the single-field inflationary models, and the constraints from CMB and LSS are relatively tighter. The future laser interferometer, DECIGO, is more effective for detecting the RGW with smaller r , but the CMB experiments, such as Planck, Clover and CMBPol, are more effective for detecting waves with larger r . They are complementary to each other for the RGW detection. The laser interferometers, as the advanced LIGO, LISA and ASTROD have less chances to find the signal of RGW, if the single-field inflationary model is held.

A final remark should be made, that is, all conclusion on RGW and their detection constraints arrived in this paper are pertinent only for single scalar field models for inflation. The RGW generated from other models of inflation need to be analyzed separately.

ACKNOWLEDGMENT: We thank S.Chongchitnan for helpful discussion. W.Zhao has been partially supported by Graduate Student Research Funding from USTC. Y.Zhang has been supported by the Chinese NSF (10173008), NKBRF (G19990754), and by SRFDP.

References

- [1] C.L.Bennett *et al.*, *Astrophys.J.Suppl.* **148** (2003) 1; D.N.Spergel *et al.*, *Astrophys.J.Suppl.* **148** (2003) 175;
- [2] G.Hinshaw *et al.*, *arXiv:astro-ph/0603451*; L.Page *et al.*, *arXiv:astro-ph/0603450*; D.N.Spergel *et al.*, *arXiv:astro-ph/0603449*;
- [3] E.M.Leitch *et al.*, *Astrophys.J.* **624** (2005) 10; C.J.MacTavish *et al.*, *arXiv:astro-ph/0507503*; J.L.Sievers *et al.*, *arXiv:astro-ph/0509203*; D.Barkats *et al.*, *Astrophys.J.* **619** (2005) L127;
- [4] S.Cole *et al.*, *Mon.Not.R.Astron.Soc.* **362** (2005) 505; M.Tegmark *et al.*, *Astrophys.J.* **606** (2005) 702; D.J.Eisenstein *et al.*, *Astrophys.J.* **633** (2005) 560;
- [5] A.Starobinsky, *JETP Lett.* **30** (1979) 682; S.Sasaki, *Prog.Theor.Phys.* **76** (1986) 1036; V.F.Mukhanov, H.A.Feldman, and R.H.Brandenberger *Phys.Rept.* **215** (1992) 203; P.J.E.Peebles, *Principles of Physical Cosmology* Princeton University Press (1993); J.A.Peacock, *Cosmological Physics* Cambridge University Press (1999); D.H.Lyth and A.Riotto, *Phys.Rept.* **314** (1999) 1;
- [6] U.Seljak and M.zaldarriaga, *Phys.Rev.Lett.* **78** (1997) 2054; M.Kamionkowski, A.Kosowsky and A.Stebbins, *Phys.Rev.Lett.* **78** (1997) 2058; J.R.Pritchard and M.Kamionkowski, *Annals Phys.* **318** (2005) 2; W.Zhao and Y.Zhang, *arXiv:astro-ph/0508345*;
- [7] <http://www.rssd.esa.int/index.php?project=Planck>;
- [8] A.C.Taylor, *et al.*, *arXiv:astro-ph/0407148*;
- [9] <http://universe.nasa.gov/program/inflation.html>; L.Verde, H.Peiris and R.Jimenez, *JCAP* **0601** (2006) 019;
- [10] <http://tamago.mtk.nao.ac.jp/>;
- [11] <http://wwwcascina.virgo.infn.it/>;
- [12] LIGO Scientific Collaboration: B.Abbott *et al.*, *Phys.Rev.Lett.* **95** (2005) 221101;

- [13] <http://www.ligo.caltech.edu/advLIGO>;
- [14] <http://lisa.nasa.gov/>;
- [15] W.T.Ni, S.Shiomi and A.C.Liao, *Class.Quant.Grav.* **21** (2004) S641;
- [16] <http://universe.nasa.gov/program/bbo.html>; V.Corbin and N.J.Cornish, *Class.Quant.Grav.* **23** (2006) 2435;
- [17] N.Seto, S.Kawamura and T.Nakamura, *Phys.Rev.Lett.* **87** (2001) 221103;
- [18] S.Detweller, *Astrophys.J.* **234** (1979) 1101; S.E.Thorsett and R.J.Dewey, *Phys.Rev.D* **53** (1996) 3468; A.N.Lommen, [arXiv:astro-ph/0208572](https://arxiv.org/abs/astro-ph/0208572);
- [19] F.Y Li, et al, *Phys.Rev.D* **62**, 044018 (2000); *Phys.Rev.D* **67**, 104008 (2003);
- [20] A.M. Cruise, *Class.Quantm Grav.* **17**, 2525 (2000); A.M. Cruise and R.M.J Ingle, *Class.Quantm Grav.* **22** S479 (2005);
- [21] Ph. Bernard et al., *Review of Scientific Instruments* **72** 2428 (2001); Ph. Bernard et al., [gr/qc-0203024](https://arxiv.org/abs/gr-qc/0203024); R. Ballantini, et al. *Class.Quantm Grav.* **20**, 3505 (2003);
- [22] Y.Zhang, Y.F.Yuan, W.Zhao and Y.T.Chen, *Class.Quant.Grav.* **22** (2005) 1383; Y.Zhang, W.Zhao, Y.F.Yuan and T.Y.Xia *Chin.Phys.Lett.* **20** (2005) 1871; Y.Zhang, X.Z.Er, T.Y.Xia, W.Zhao and H.X.Miao, *Class.Quant.Grav.* **23** (2006) 3783;
- [23] B.Allen, [arXiv:gr-qc/9604033](https://arxiv.org/abs/gr-qc/9604033); R.H.Cyburt, J.Ellis, B.D.Fields and K.A.Olive, *Phys.Rev.D* **67** (2003) 103521; R.H.Cyburt, B.D.Fields, K.A.Olive and E.Skillman, *Astropart.Phys.* **23** (2005) 313; T.L.Smith, E.Pierpaoli and M.Kamionkowski, [arXiv:astro-ph/0603144](https://arxiv.org/abs/astro-ph/0603144);
- [24] M.Maggiore, *Phys.Rept.* **331** (2000) 283;
- [25] E.W.Kolb and M.Turner, *The Early Universe* Addison-Sesley Publishing Company (1990);
- [26] S.Weinberg, *Phys.Rev.D* **69** (2004) 023503; D.A.Dicus and W.W.Repko, *Phys.Rev.D* **72** (2005) 088302;
- [27] L.A.Boyle and P.J.Steinhardt, [arXiv:astro-ph/0512014](https://arxiv.org/abs/astro-ph/0512014);
- [28] C.G.Tsagas and J.D.Barrow, *Class.Quant.Grav.* **14** (1997) 2539; C.G.Tsagas and R.Maartens, *Phys.Rev.D* **61** (2000) 083519;
- [29] A.R.Liddle and D.H.Lyth, *Phys.Lett.B* **291** (1992) 391; A.R.Liddle and D.H.Lyth, *Phys.Rep.* **231** (1993) 1;
- [30] U.Seljak, A.Slosar and P.McDonald, [arXiv:astro-ph/0604335](https://arxiv.org/abs/astro-ph/0604335);
- [31] T.L.Smith, M.Kamionkowski and A.Cooray, *Phys.Rev.D* **73** (2006) 023504; S.Chongchitnan and G.Efstathiou, *Phys.Rev.D* **73** (2006) 083511; T.L.Smith, H.V.Peiris and A.Cooray, *Phys.Rev.D* **73** (2006) 123503;
- [32] M.S.Turner, M.White and J.E.Lidsey, *Phys.Rev.D* **48** (1993) 4613;
- [33] J.C.Fabris, S.V.B.Goncalves and M.S. dos Santos, *Gen.Rel.Grav.* **36** (2004) 2559; M.S.Santos, S.V.B.Goncalves, J.C.Fabris and E.M.de Gouveia Dal Pino, [arXiv:gr-qc/0504032](https://arxiv.org/abs/gr-qc/0504032);
- [34] B.Kampfer, *Annalen Phys.* **9** (2000) 605; D.J.Schwarz, *Annalen Phys.* **12** (2003) 220; T.Schaefer, [arXiv:hep-ph/0509068](https://arxiv.org/abs/hep-ph/0509068);
- [35] Y.Watanabe and E.Komatsu, *Phys.Rev.D* **73** (2006) 123515 ;
- [36] D.J.Schwarz, *Mod.Phys.Lett.A* **13** (1998) 2771;
- [37] L.P.Grishchuk, *Zh.Eksp.Teor.Fiz.* **67** (1974) 825; L.P.Grishchuk, *Ann. NY Acad.Sci.* **302** (1977) 439; L.P.Grishchuk, V.M.Lipunov, K.A.Postnov, M.E.Prokhorov and B.S.Sathyaprakash, *Phys.Usp.* **44** (2001) 1;
- [38] M.Zaldarriaga and U. Seljak, *Phys.Rev.D* **58** (1998) 023003; M. Kesden, A. Cooray and M. Kamionkowski *Phys.Rev.Lett.* **89** (2002) 011304 ; L. Knox and Y. S. Song, *Phys.Rev.Lett.* **89** (2002) 011303; W.Hu, M.M.Hedman and M.Zaldarriaga, *Phys.Rev.D* **67** (2003) 043004;
- [39] S.Dodelson, W.H.Kinney and E.W.Kolb, *Phys.Rev.D* **56** (1997) 3207; W.H.Kinney, *Phys.Rev.D* **58** (1998) 123506; H.V.Peiris *et al.*, *Astrophys.J.Suppl.* **148** (2003) 175;
- [40] L.Alabidi and D.Lyth, *JCAP* **0605** (2006) 016; L.Alabidi and D.Lyth, [arXiv:astro-ph/0603539](https://arxiv.org/abs/astro-ph/0603539);

- [41] M.B.Hoffman and M.S.Turner, Phys.Rev.D **64** (2001) 023506; W.H.Kinney, Phys.Rev.D **66** (2002) 083508; A.R.Liddle, Phys.Rev.D **68** (2003) 103504; S.Chongchitnan and G.Efstathiou, Phys.Rev.D **72** (2005) 083502;
- [42] W.H.Kinney, Phys.Rev.D **66** (2002) 083508; R.Easter and W.H.Kinney, Phys.Rev.D **67** (2003) 043511;
- [43] E.J.Copeland, A.R.Liddle and D.Wands, Phys.Rev.D **57** (1998) 4686;
B.Gumjudpai, T.Naskar, M.Sami and S.Tsujikawa, JCAP **0506** (2005) 007;
- [44] A.R.Liddle, P.Parsons and J.D.Barrow, Phys.Rev.D **50** (1994) 7222;
- [45] E.D.Stewart and D.H.Lyth, Phys.Lett.B **302** (1993) 171;
- [46] U.Seljak *et al.*, Phys.Rev.D **71** (2005) 103515;

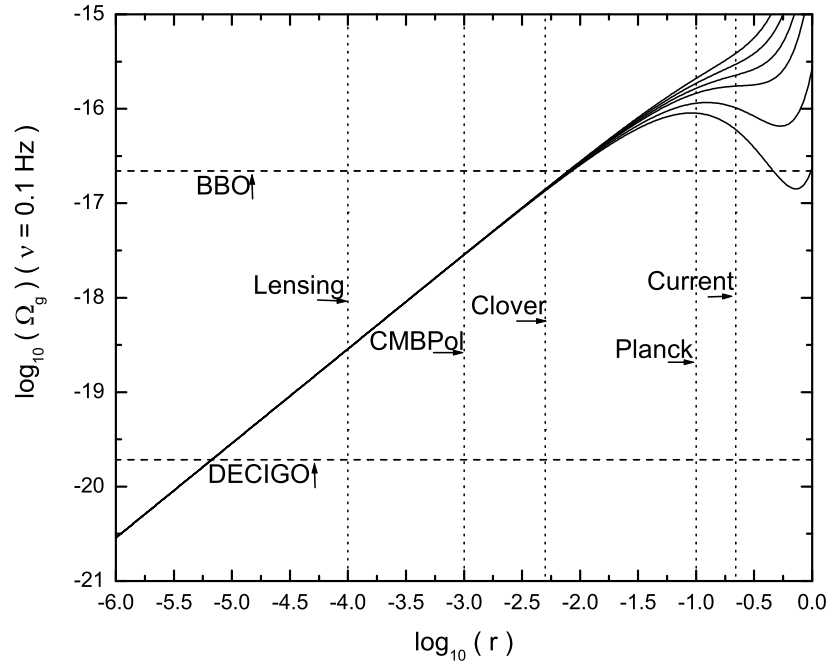


Figure 1: The strength of RGW at $\nu = 0.1\text{Hz}$ depends on the slow-roll parameters n_s and r . This figure shows the results of analytic approximation in (25). The solid lines from top down are the curves with $n_s = 1.00, 0.98, 0.96, 0.94, 0.90, 0.86$, respectively. The vertical (dot) lines from right to left are the sensitive limit curves of current observations, Planck, Clover, CMBPol, and the sensitive limit of CMB observations, respectively. The horizontal (dash) lines from up to down are the sensitive limit curves of BBO and DECIGO, respectively.

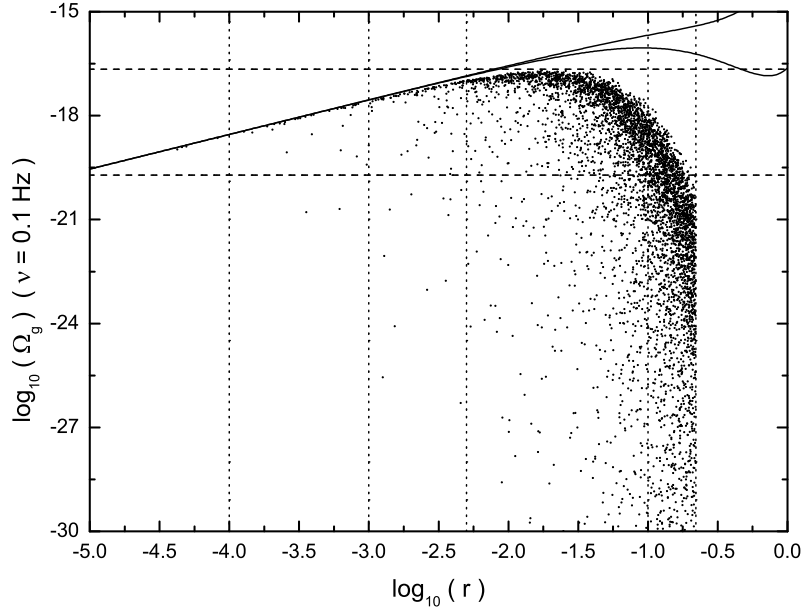


Figure 2: The distribution of the 5509 realizations in the $r - \Omega_g$ plane. The solid lines from top down are the analytic curves with $n_s = 1.00$ and $n_s = 0.86$, respectively. The vertical (dot) lines and the horizontal (dash) lines have the same meanings with which in Fig.[1].

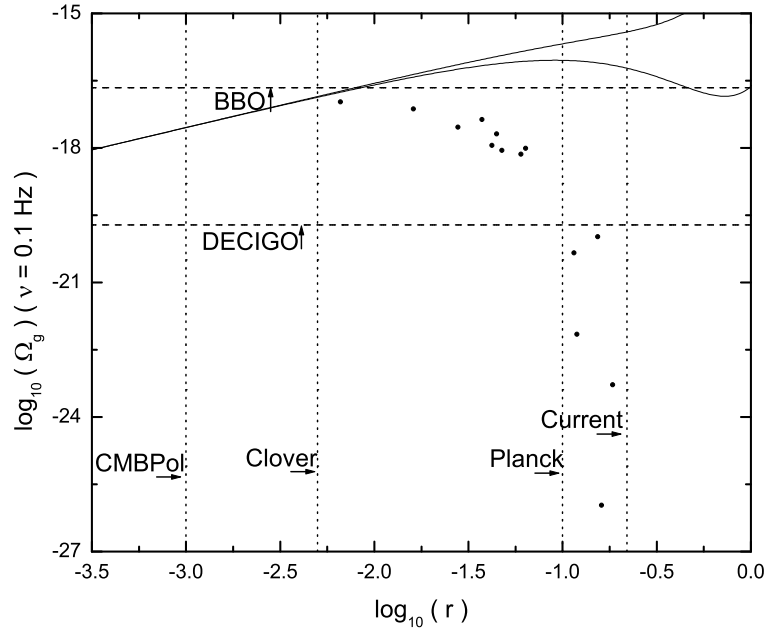


Figure 3: The distribution of the 14 realizations in the $r - \Omega_g$ plane. The solid lines from top down are the analytic curves with $n_s = 1.00$ and $n_s = 0.86$, respectively. The vertical (dot) lines from right to left are the sensitive limit curves of current observations, Planck, Clover and CMBPol, respectively. The horizontal (dash) lines from up to down are the sensitive limit curves of BBO and DECIGO, respectively.